Photoconductivity of CdTe nanocrystal films in a simple multilayer device structure

2008 J. Phys.: Condens. Matter 20 385206

(http://iopscience.iop.org/0953-8984/20/38/385206)

J. Phys.: Condens. Matter **20** (2008) 385206 (6pp) doi:10.1088/0953-8984/20/38/385206

Photoconductivity of CdTe nanocrystal films in a simple multilayer device structure

R S Aga Jr, D Jowhar, M Ewan, A Steigerwald, A Ueda, Z Pan, W E Collins and R Mu

Center for Physics and Chemistry of Materials, Fisk University, Nashville, TN 37208, USA

E-mail: raga@fisk.edu

Received 18 June 2008, in final form 6 August 2008
Published 27 August 2008
Online at stacks.iop.org/JPhysCM/20/385206

Abstract

The photoconductivity of CdTe nanocrystal films was investigated by employing a ZnO/CdTe/In multilayer device structure. CdTe was deposited on a ZnO electrode by a pulsed electron-beam technique at argon background gas pressures of 9, 13 and 17 mTorr. Using two photo-excitation sources (visible and near-infrared), the device with the CdTe deposited at 17 mTorr demonstrated the highest photocurrent to dark current ratio, suggesting the highest quantum efficiency among the three different devices. It also demonstrated the highest short circuit photocurrent and the fastest photocurrent decay. These results are attributed to the formation of more nanocrystals at 17 mTorr with enhanced optoelectronic properties.

(Some figures in this article are in colour only in the electronic version)

1. Introduction

CdTe is a technologically important material with major applications in solar energy conversion and photodetection. With its bulk bandgap energy (E_g) of ~1.5 eV (~820 nm), CdTe thin film solar cells are ideal for large area and low cost terrestrial photovoltaic systems. They have achieved power conversion efficiencies up to 16.2% [1] but this is still far from their theoretical photovoltaic conversion efficiency, which is around 28%. Clearly, there are still some issues that need further understanding to obtain efficiencies closer to the theoretical limit. One of which is the role of grain boundaries (GBs) in the film. There are several thin film polycrystalline solar cells that significantly outperform their single-crystal counterpart [2]. GBs limit photocurrent transport in the films but it has been reported that they can also enhance the dissociation of electron–hole (e–h) pairs, which improves photocurrent collection along GBs [3]. This competing mechanism suggests that there may exist an optimum CdTe morphology where the limiting effect of GBs is minor as compared to the improvement in the efficiency due to the enhanced e–h dissociation along the GBs. A similar argument arises between a smooth film with reduced GBs versus a nanocrystal film with a large number of interparticle GBs. The smooth film will have better electrical conductivity but the nanocrystals, which have been observed to exhibit larger absorption coefficients [4], are expected to have higher quantum efficiency (QE).

To experimentally address these issues, a method to fabricate CdTe nanocrystal film with controllable morphology is desirable. This may be achieved by controlling the nanoparticle formation during the deposition so that morphology can vary from smooth films (less GBs) to nanocrystal films consisting of many nanoparticles (more GBs). However, with the mature techniques to fabricate CdTe films such as vacuum evaporation, electrolytic deposition, spray pyrolysis, atomic layer epitaxy and closed-spaced sublimation [5], control of morphology is fairly difficult and most often post-deposition thermal annealing, which can modify GB chemistry and properties, is necessary. Therefore, it is worthwhile to explore other techniques to fabricate CdTe nanocrystal films with controllable morphology and investigate the photoconductivity of such films in a multilayer device structure similar to solar cells and photodetectors. In addition, such techniques can be extended to fabricate nanostructured semiconductors, which have received appreciable attention recently due to their unique properties. For example, CdTe nanorods, tetrapods and nanoparticles have been explored in organic–inorganic active layers for hybrid solar cells [6–8].

The dependence of E_g to the semiconductor dimension due to quantum confinement effects can be exploited to achieve optimum sunlight absorption and power conversion efficiency. Semiconducting nanocrystals exhibiting quantum confinement effects are very attractive for photosensitization of wide band gap semiconductors [9, 10] because they have enhanced QE. In fact, multiple exciton generation and electrical extraction from a PbSe nanocrystal photoconductor has already been reported [11].

In this work, it is demonstrated that pulsed electron-beam deposition (PED) is an attractive technique to deposit CdTe nanocrystal films with varying morphology. By investigating the photoconductivity in these films, it was observed that the film with the largest number of nanocrystals had the highest photocurrent to dark current ratio (γ) indicative of high QE of the nanocrystals. It also exhibited the highest short-circuit photocurrent (I_{SC}), which suggests that the grain connectivity in the CdTe film prepared by PED is not a major concern so its current limiting effect may be masked by other mechanisms such as the enhanced charge carrier generation in the nanocrystals and efficient charge separation along the GBs. This is an important result because in the applications of CdTe for solar energy conversion or photodetection, efficient generation of e–h pairs in the CdTe and the subsequent electrical extraction, are key to achieve high device performance.

2. Experiment

A commercial CdTe target was employed for PED. In all depositions, the following parameters were fixed: (a) target-to-substrate distance: 50 mm, (b) average electron energy: 15 keV, (c) repetition rate: 2 Hz (d) pulsed width: 100 ns and (e) substrate temperature: 300 K. Argon was employed as the background gas. To vary the morphology of CdTe films, three values of background gas pressure (P_B) were selected. For convention, CdTe samples that were deposited at 9, 13 and 17 mTorr were referred to as S-9, S-13 and S-17 respectively. They were deposited on several mica and silicon substrates for AFM (atomic force microscopy), SEM (scanning electron microscopy) and RBS (Rutherford backscattering spectroscopy) analysis. Similarly, devices prepared at 9, 13 and 17 mTorr were labeled as D-9, D-13 and D-17 respectively. They were prepared on several glass substrates pre-coated with a 150 nm-thick ZnO film. CdTe was deposited on the middle region of the ZnO film using a mask. It should be mentioned that since the deposition rate varies with P_B, the number of pulses was adjusted accordingly based on prior calibration. This maintained comparable thickness of CdTe film for each device. The CdTe film was sandwiched between the ZnO and Indium (In) electrodes to form a simple ZnO/CdTe/In multilayer device structure. The In back electrode (area $\sim 1.5 \times 1.5$ mm^2) was pressed on the CdTe film. This contacting method was tested several times to ensure consistent device performance. Electrical characterization was performed using a Keithley 2400 sourcemeter. Two different light sources were used to provide photo-excitation of the devices at visible and near-infrared (NIR) wavelengths. One was a 632 nm laser and the other one was a halogen lamp equipped with a long wave pass filter with cutoff at 760 nm. At the position of the device, the power density of the two different illuminations was set to ~ 2 mW cm^{-2}. In the measurement, light was incident on the ZnO-coated substrate. Bias on the devices was swept from -1.5 V to $+1.5$ V. NIR photocurrent decay of the devices at a constant bias of -1 V was also characterized. Finally, a UV–visible–NIR spectrophotometer was employed to measure the optical transmittance of the devices in the wavelength range of 300–1000 nm.

3. Results and discussion

SEM images of the CdTe films deposited on silicon wafer are shown in figures 1(a)–(c). All of them have isolated particles bigger than 50 nm but among the three, S-9 has the smoothest surface with few nanoparticles smaller than 20 nm. For S-13, there seems to be clustering of nanoparticles as indicated by the bright-looking islands. S-17 features the largest number of nanoparticles on the surface. These observations are consistent with the AFM analysis. Using just 100 pulses, a reasonable number of isolated nanoparticles were collected on mica substrate for particle size measurement. The results are shown in figures 1(d) and (e). S-17 exhibits the highest number of nanoparticles per unit area ($\sim$25.6 particles μm^{-2}) but with the smallest dominant particle size of 1–2 nm. S-13 has the second highest nanoparticle density ($\sim$15.2 particles μm^{-2}) with a dominant particle size of 7–8 nm. For S-9, it was extremely difficult to find a measurable particle distribution. This suggests that the deposition at 9 mTorr is dominated by smooth film formation consistent with figure 1(a). Based on AFM and cross-sectional SEM analysis, it is likely that CdTe deposition at these P_B values yields a mixture of smooth film and nanocrystals. The smooth film constituent decreases as the nanocrystal formation takes place. Thus, S-9 has more smooth film constituent but lesser number of nanocrystals as compared to S-13 while S-17 has the least amount of smooth film constituent but the highest number of nanocrystals. This interpretation is in agreement with the images in figure 1. It is worthwhile to mention that the explanation for the decrease in particle size due to P_B increase has been reported on the PED of YBCO precursors [12]. Using RBS, the Cd to Te ratio for all the samples was determined to be 1 within experimental uncertainty. This indicates that at the selected P_B values, the ablation and deposition of the Cd and Te species is congruent.

The setup for the device characterization is depicted in figure 2(a). The thickness of the CdTe film was $\sim$500 nm and the sheet resistance of the ZnO electrode was $\sim$300 kΩ/square. Figure 2(b) represents a typical dark I–V curve of the device. In this measurement, the In electrode was positive at forward bias. The curve reflects two basic processes in the device: (a) injection of charge carriers from the electrodes into the CdTe film and vice versa and (b) transport of the carriers in the film. Since there are two junctions in the device (ZnO/CdTe and CdTe/In), the current exhibits exponential increase with either forward or reverse bias. The presence of an energy barrier at each interface causes the current in the device to have a nonlinear voltage dependence in both directions. At forward

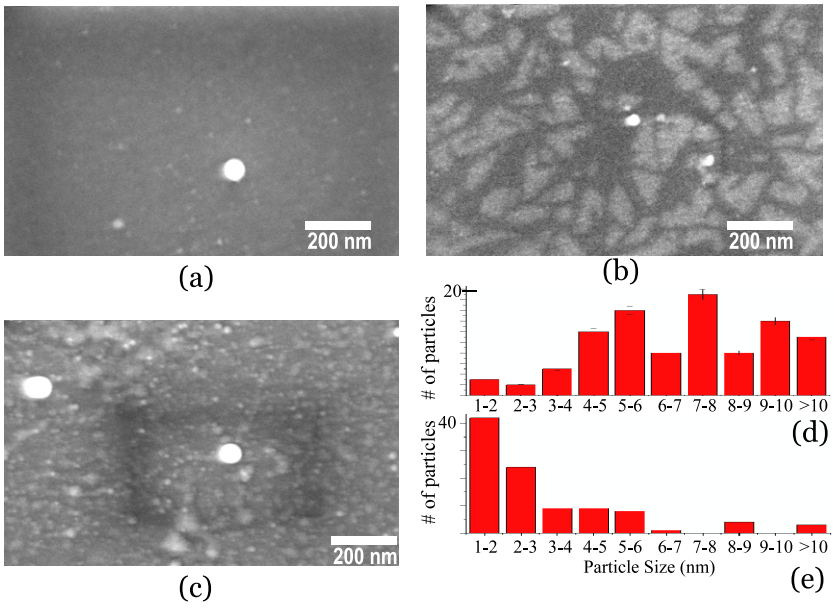

Figure 1. Scanning electron microscope images of CdTe nanocrystal film deposited on silicon wafer by a pulsed electron deposition technique at argon background gas pressures of (a) 9 mTorr, (b) 13 mTorr and (c) 17 mTorr. Nanoparticle size distribution analysis for CdTe deposited on mica under (d) 13 mTorr and (e) 17 mTorr.

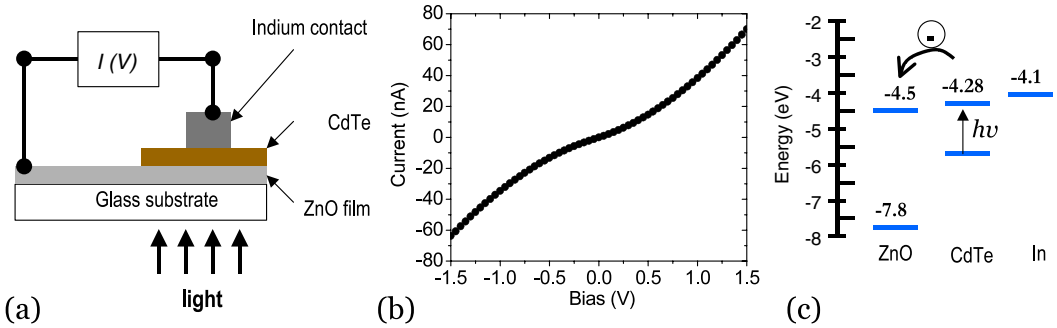

Figure 2. (a) Device structure and measurement setup. (b) Representative dark I–V curve of the device and its (c) energy level diagram.

bias, the current in the device is limited by the ZnO/CdTe interface. Electron injection from ZnO to CdTe is hindered by the large barrier that is formed when CdTe is biased at higher potential than ZnO. On the other hand, electron injection from CdTe to In only encounters a small barrier due to the lowering of the Fermi energy of the In with respect to the Fermi energy in the CdTe. At reverse bias, the electron barrier at ZnO/CdTe is lowered while the larger barrier is formed at the CdTe/In interface. This hinders the electron injection from In to CdTe and thus limit the current in the device. Figure 2(c) shows the energy level diagram of the device. It can be seen that the photogenerated electrons in the CdTe can transfer to the ZnO. Thus, the reverse bias I–V curve reflects the behavior of the ZnO as an electron acceptor, which is relevant for photovoltaics. Due to its relevance, the reverse bias I–V curve was chosen for the analysis of photoconductivity. It should be mentioned that previous experiments also demonstrated that the photogenerated electrons in CdTe quantum dots could transfer to the ZnO nanowires [10]. This was verified in this work when the direction of the measured I_{SC} in these devices was observed to flow from ZnO to CdTe.

Figure 3 shows the I–V curves of the three devices at reverse bias. For convenience, the absolute values of the current and the bias are displayed in the figure. The black closed-square symbols represent the dark I–V. Over the entire bias range, the lowest dark current is exhibited by D-17 followed by D-13 and then D-9. This is consistent with the previous observation that S-17 had the largest number of nanocrystals and the least smooth film constituent. Thus, D-17 is expected to have the highest amount of GBs, which suppress the dark current. On the other hand, D-9 exhibits the highest dark current because it is expected to consist mostly of smooth film with only few nanocrystals similar to S-9. For photodetection, one of the most important parameters is the photocurrent to dark current ratio γ. For a semiconductor sandwiched by two Ohmic contacts, γ is determined by the increase of the charge carrier density (n) in the conduction band, which makes it independent of the bias voltage. Thus, it is an indirect measure of QE. In figure 3, the open-circle and closed-circle symbols correspond to I–V under NIR and 632 nm photo-excitation respectively. To examine whether a

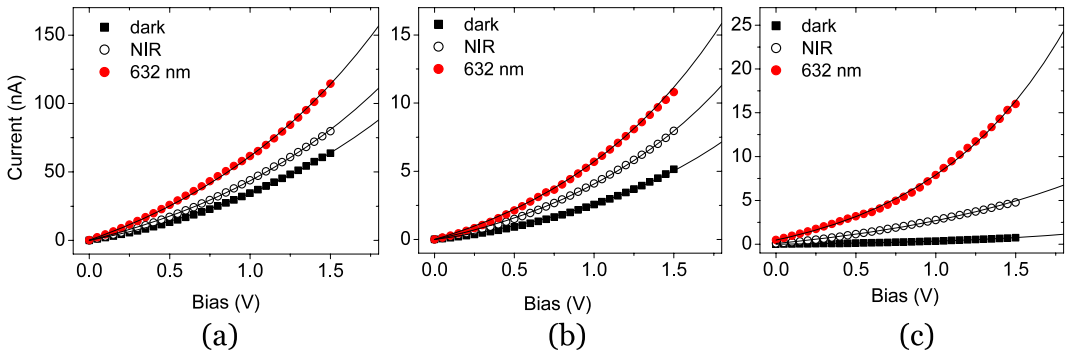

Figure 3. I–V curves of devices (a) D-9, (b) D-13 and (c) D-17 under different photo-excitations.

bias independent γ could be assumed for the ZnO/CdTe/In devices in the bias range of 0 down to −1.5 V, two functions, labeled here as $I_D(V)$ and $I_P(V)$ which fit well to the dark and photo-excited I–V curves respectively were determined. If the ratio of these two functions is constant, then γ is bias independent and its average is simply $I_P(V)$ divided by $I_D(V)$. It was found that a diode-like equation of the form:

$$I(V) = I_0[e^{(\alpha|V|)} - 1] \tag{1}$$

could fit fairly well to the experimental I–V curves with the appropriate values of the parameters I_0 and α. Moreover, for each device a single value of α could be used to represent the dark and the photo-excited I–V curves. With a constant α, only the value of I_0 changes under different photo-excitation. Thus, the average γ can be expressed as:

$$\gamma = \frac{I_P(V)}{I_D(V)} = \frac{I_{0P}}{I_{0D}} \tag{2}$$

where I_{0P} and I_{0D} are the values of the parameterI_0 in the dark and under photo-excitation respectively. These findings reveal that γ is indeed constant in bias range of 0 down to −1.5 V. They also indicate that γ is mainly determined by the increase of n in the CdTe nanocrystal film. However, the presence of small I_{SC} also suggests a weak photovoltaic effect. In figures 3(a)–(c), the quality of the fittings (solid curve) is illustrated. From the analysis, the corresponding α values are 0.75, 0.9 and 1.15 for D-9, D-13 and D-17 respectively. Under NIR and 632 nm, γ values are 1.26 and 1.78 respectively for D-9. For D-13, γ values are 1.58 and 2.21 respectively. The slightly higher γ for D-13 is attributed to its higher number of CdTe nanocrystals, which have been reported to exhibit higher absorption coefficients as compared to their smooth thin film counterpart [4]. This interpretation is further supported by D-17, which has γ values of 15.9 and 21.2 under NIR and 632 nm respectively. This device demonstrates the highest QE among the three because it has the highest number of nanocrystals. In fact, results from optical transmission measurement of the devices revealed that D-17 has the largest number of nanocrystals that exhibit quantum confinement effects. The enhanced QE of the nanocrystals results to the increase of γ in D-17 by approximately a factor of 10. In addition, the increase in photocurrent when photo-excitation source was switched from NIR to 632 nm while maintaining intensity was highest for D-17. The difference in γ values corresponding to 632 nm and NIR photo-excitation, which yields the photocurrent increase normalized by the dark current was 5.3, 0.6 and 0.5 for D-17, D-13 and D-9 respectively. The increase in photocurrent under 632 nm photo-excitation, is attributed to the generation of e–h pairs in the CdTe nanocrystals with band edge absorption below 760 nm but above 632 nm. Thus, they exhibit photoconductivity under 632 nm but not under NIR. Based on this interpretation, D-17 should have the highest number of such nanocrystals followed by D-13 and D-9. Again, this is in agreement with the SEM and AFM analysis. When the I_{SC} of the devices at 632 nm was compared, D-17 demonstrated the highest value at 0.5 nA as compared to 0.25 nA for D-9 and almost zero for D-13. This implies that the current limiting effect of GBs may be masked by other mechanisms in the film such as the enhanced QE of the nanocrystals.

Results from NIR photocurrent decay measurements also showed that D-17 exhibits the fastest decay implying the least number of hole traps that slows down electron–hole recombination rate. The normalized photocurrent decay curves of the three devices are depicted in figures 4(a)–(c). They are observed to comprise of two major processes. After turning off the light, the decay was fast at first and then it slowed down. Thus, the normalized photocurrent decay was modeled by a sum of two-exponentially decaying functions of the form:

$$I_n(t) = A\,e^{-t/\tau_1} + B\,e^{-t/\tau_2} \tag{3}$$

where τ_1 and τ_2 are two characteristic time constants representing a fast and a slow decay respectively. The former is generally attributed to bulk-related processes while the latter is due to surface-related processes. In the normalization, the current at $t = 0$, which is the steady state photocurrent, is set to 1 and this decays to the dark current value, which is set to 0. In all the devices, the timescale for this decay was under 10 min. The coefficients A and B, where $A + B = 1$, represent weighing factors that quantify the relative contribution of each mechanism to the decay process. It can be observed from figures 4(a)–(c) that this model fits nicely to the experimental data. Figure 4(d) compares the curves that best fit the photocurrent decay of the three devices. They are plotted in a logarithmic scale to show clearly the two major decay rates as indicated by the two different slopes in the curve. It can be

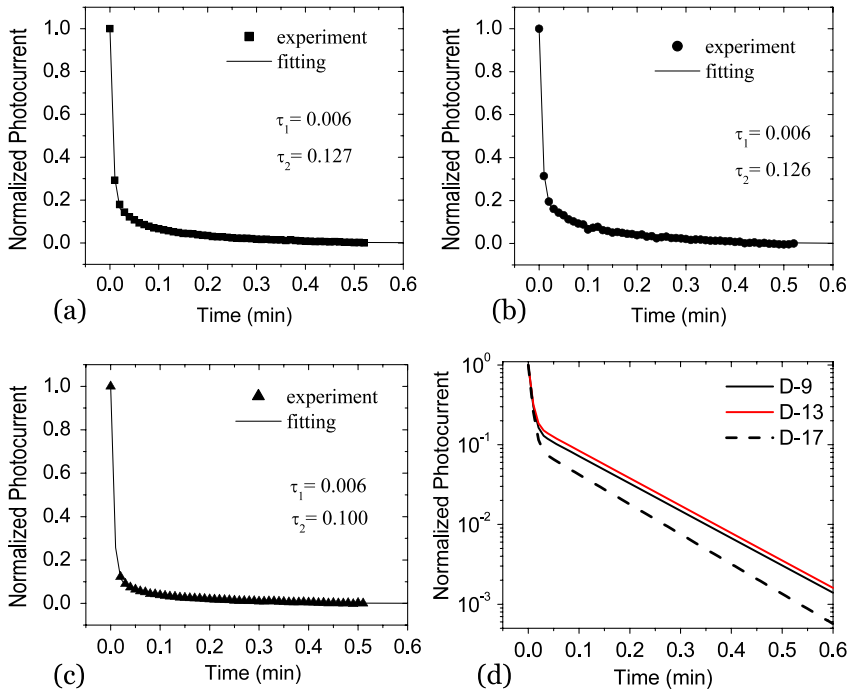

Figure 4. Normalized photocurrent decay of devices (a) D-9, (b) D-13 and (c) D-17 after the near-infrared photo-excitation source is turned off. The solid curve is the best fit using the two-exponentially decaying function. (d) Comparison of the fitted curves for the three devices in log scale.

noticed that the fast decay process is similar for all the devices. However, the slow decay of D-17 deviates significantly from that of D-9 and D-13. It was indeed found that the value of τ_1 was 0.36 s for all of them. However, the value of B was ∼0.1 for D-17 and ∼0.2 for D-9 and D-13. It implies that the surface-related photoconduction in D-17 is lesser as compared to D-9 and D-13. This is supported by the lower τ_2 value of D-17 (6.00 s) as compared to D-9 (7.62 s) and D-13 (7.56 s). These results demonstrate that the nanocrystals and the associated interparticle GBs in D-17 do not provide significant hole traps that slow down photocurrent decay in the device. This is evidenced by the low τ_2 value of D-17 despite having the largest number of GBs. In contrast, D-9, which consists of the smoothest CdTe film among the three devices, has the longest τ_2 value of 7.62 s. Thus, in the PED-prepared CdTe nanocrystal films, the significant hole trapping processes are due to the smooth film constituent that form on the ZnO surface and not from the nanoparticles that are collected by the ZnO electrode. The smooth CdTe film constituent on the ZnO surface is likely dominated by a wurtzite (WZ) phase, which is expected to have more hole traps based on first-principles calculations [13]. Previous studies have shown that CdTe can exist in cubic zinc blende (ZB) and WZ crystal structures. Furthermore, the energy difference between these two phases is small [14]. As a result, the metastable WZ phase, which usually exists as a contaminant in equilibrium ZB CdTe films, may have been formed favorably on the ZnO, which is a WZ crystal. In the case of the CdTe nanoparticles that form in the background gas, they have already a defined crystal structure, which is likely dominated by equilibrium ZB, before they land on the ZnO surface to form the nanocrystal film. Thus, D-17 features the fastest photocurrent decay because it consists of the largest number of nanocrystals with ZB phase. In contrast, D-9 features the slowest photocurrent decay because it mainly consists of smooth film with WZ phase. It should be realized that the hole traps did not degrade the electrical conductivity of the CdTe films in this work because they were n-type. This interpretation is further supported by the faster photocurrent decay in ITO/CdTe/In devices. By replacing ZnO with ITO, which has a cubic crystal structure, it was observed that both τ_1 and τ_2 became faster for the three devices while the trend in γ was maintained. For the case of D-17, τ_1 and τ_2 decreased from 0.36 s and 6.00 s to 0.18 s and 4.8 s respectively.

4. Conclusion

Pulsed electron deposition has been employed to deposit CdTe on ZnO electrode. The morphology of CdTe was varied by deposition under different Ar background gas pressures. At P_B values of 9, 13 and 17 mTorr, CdTe nanocrystal films were formed. They consisted of a mixture of smooth film and nanocrystals. The presence of nanocrystals reduced the dark current but increased γ due to their higher QE. In contrast, the smooth film constituent that formed on the ZnO surface increased the dark current and slowed down the photocurrent decay due to its possible WZ phase, which acts as hole traps. Among all the devices, the one with CdTe deposited at 17 mTorr had the highest number of nanocrystals and the least amount of smooth film constituent. Consequently, it exhibited the highest γ, the highest I_{SC} and the fastest photocurrent decay.

Acknowledgments

This research is supported in part by NSF-CBET-0829977, NREL/DOE ACQ-4-33623-03 and NSF-CREST CA:HRD-0420516 and NSF-STC CliPS under grant No. 0423914. A portion of this research was conducted at the Center for Nanophase Materials Sciences, which is sponsored at Oak Ridge National Laboratory by the Division of Scientific User Facilities, US Department of energy.

References

[1] Paulson P L and Dutta V 2000 *Thin Solid Films* **10** 299
[2] Moller H J 1993 *Semiconductors for Solar Cells* (Boston, MA: Artech House Publishers)
[3] Herndon M K, Gupta A, Kaydanov V and Collins R T 1999 *Appl. Phys. Lett.* **75** 3503
[4] Mastai Y and Hodes G 1997 *J. Phys. Chem.* B **101** 2685
[5] Chung G Y, Park S C, Cho K and Ahn B T 1995 *J. Appl. Phys.* **78** 5494
[6] Kang Y, Park N and Kim D 2005 *Appl. Phys. Lett.* **86** 113101
[7] Gur I, Fromer N A and Alivisatos A P 2006 *J. Phys. Chem.* B **110** 25543
[8] Kumar S and Nann T 2004 *J. Mater. Res.* **19** 1990
[9] Zaban A, Micic O I, Gregg B A and Nozik A J 1998 *Langmuir* **14** 3153
[10] Aga R S Jr, Jowhar D, Ueda A, Pan Z, Collins W E, Mu R, Singer K D and Shen J 2007 *Appl. Phys. Lett.* **91** 232108
[11] Kim S J, Kim W J, Sahoo Y, Cartwright A N and Prasad P N 2008 *Appl. Phys. Lett.* **92** 031107
[12] Mathis J E and Christen H M 2007 *Physica* C **459** 47
[13] Yan Y, Al-Jassim M M, Jones K M, Wei S H and Zhang S B 2000 *Appl. Phys. Lett.* **77** 1461
[14] Neretina S, Mascher P, Hughes R A, Braidy N, Gong W H, Britten J F, Preston J S, Sochinskii N V and Dippo P 2006 *Appl. Phys. Lett.* **89** 133101